Construction and Building Materials 407 (2023) 133566

Contents lists available at ScienceDirect

Construction and Building Materials

journal homepage: www.elsevier.com/locate/conbuildmat

New insights on understanding the Portland cement hydration using electrical impedance spectroscopy

M. Bortoletto [a], A.O. Sanches [a,*], J.A. Santos [a], R.G. da Silva [a], M.M. Tashima [a,b,*], J. Payá [b], L. Soriano [b], M.V. Borrachero [b], J.A. Malmonge [a], J.L. Akasaki [a]

[a] Universidade Estadual Paulista (UNESP), Faculdade de Engenharia, Grupo de Pesquisa MAC - Materiais Alternativos de Construção, Campus de Ilha Solteira, São Paulo, Brazil

[b] Instituto de Ciencia y Tecnología del Hormigón – ICITECH. Grupo de investigación en Química de los Materiales – GIQUIMA, Universitat Politècnica de València (UPV), Spain

ARTICLE INFO

Keywords:
Impedance spectroscopy
Portland cement hydration
Electrical properties
Setting time

ABSTRACT

This study aimed to bring new perspectives and understandings, as well as to elucidate the behavior of Portland cement hydration through electrical conductivity curves obtained by impedance spectroscopy (IS). The IS measurement was performed on Portland cement paste with w/c ratio of 0.40 up to 28 curing days. According to the results, based on the inflection points of its respective derivative, the electrical conductivity curve of Portland cement paste can be subdivided into eight different regions. A new region (region IV) in the acceleration period, characterized by the resume of dissolution reactions and microstructure formation with the paste in a semi-fluid state, was established. Moreover, a shoulder observed in region VI was attributed to the formation of AFt phases from the reduction of $CaSO_4$, and secondary reactions of ionic release in the pore network. Hence, new insights on the electrical conductivity curve of Portland cement paste are reported confirming the IS as a sensitive and promising technique.

1. Introduction

Portland cement is the most widely used binder in the world, with an estimated global production of more than 4 Gt per year [1]. Portland cement hydration is a complex exothermic reaction among clinker compounds, calcium sulfate, mineral admixtures, and water. As well known, this reaction is directly influenced by several factors such as the phase composition of the clinker, the presence of ions in the crystalline network of the clinker compounds, fineness, hydration temperature, water/binder ratio, conditions curing, etc [2].

Since its invention in 1824 by Joseph Aspdin, extensive efforts have been made to understand the Portland cement hydration process [3,4]. Most instrumental techniques employed for this purpose are time-consuming and expensive [5–10], while others are destructive and present limited information [11]. Among these techniques, isothermal calorimetry is the most used to assess Portland cement hydration due to its accessibility [3,12,13]. According to the literature, five main stages are stated using this technique: dissolution, induction, acceleration, deceleration, and continuous slow hydration [1,14]. However, the lack of sensitivity of isothermal calorimetry to low heat variations, especially for the induction period, does not allow an in-deep understanding of hydration reactions and, consequently, microstructure formation [15].

In this sense, in 1988, McCarter et al. [16] proposed the application of electrical impedance spectroscopy (IS) to assess Portland cement hydration. Very promising results demonstrated that IS could be a simple, low-cost, and powerful non-destructive technique, mainly due to its high sensitivity compared to isothermal calorimetry [17–19]. A correlation between isothermal calorimetry and IS measurements in cementitious materials was presented in several works [20–23]. The complex hydration reactions, microstructural changes, and the different hydration regions can be identified from the IS, indicating its efficiency with respect to isothermal calorimetry.

In the last decades, numerous works using IS have been carried out to interpret the complex/undefined reactions involved in the hydration of Portland cement [17,20,24–32]. Huang et al. [32] evaluated the evolution of the microstructure of Portland cement pastes during the fresh state from the IS. The authors identify, through electrical resistivity measurements, two inflection points in the bulk resistivity curve and

* Corresponding authors at: Universidade Estadual Paulista (UNESP), Faculdade de Engenharia, Grupo de Pesquisa MAC - Materiais Alternativos de Construção, Campus de Ilha Solteira, São Paulo, Brazil.

E-mail addresses: alex.o.sanches@unesp.br (A.O. Sanches), maumitta@upvnet.upv.es (M.M. Tashima).

https://doi.org/10.1016/j.conbuildmat.2023.133566
Received 26 July 2023; Received in revised form 15 September 2023; Accepted 26 September 2023
Available online 29 September 2023

Table 1
Chemical composition of Portland cement (CPV) (%, by mass).

Compound	Mass content (%)
CaO	62.77
SiO_2	19.90
Al_2O_3	4.40
Fe_2O_3	4.59
MgO	1.15
Na_2O	0.10
K_2O	0.96
SO_3	1.63
Others	0.19
LOI	4.31
C_3S	57.79
C_2S	8.30
C_3A	3.54
C_4AF	12.70
Calcium Carbonate (%)	9.04

three different regions in the Portland cement hydration process during the setting. The first region showed a reduction in bulk resistivity and corresponded to the initial period of hydration, and changes in microstructure were attributed to the flocculation of Portland cement particles. The second region was characterized by an increase in bulk resistivity and represents the induction period of Portland cement, in which changes in microstructure were still attributed to flocculation of cement particles. The third region showed an exponential increase in bulk resistivity, represented by the rapid formation and growth of hydrated products in the pore network leading to paste rigidity.

Schwarz et al. [28] used IS in the characterization of cement pastes with glass powder incorporation (10–30 wt%) and concluded that from the electrical conductivity curve and its derivative, it was possible to identify five hydration regions corresponding to the stages of dissolution, induction, acceleration and deceleration and a steady state, showing similarities with the periods obtained from a typical curve of heat evolution.

Sanish et al. [20] used IS to monitor the early hydration process and porosity in cementitious materials containing mineral additions (limestone, fly ash, and silica fume). Four different hydration regions were identified from the electrical conductivity curve and its derivative, comprising the periods of dissolution, induction, acceleration, and deceleration/steady state of the hydration process. Furthermore, the initial and final setting time of cement pastes were predicted and compared with the values obtained in the Vicat test. The maximum deviation of 5% of the values between the two methods was obtained, showing that the IS is an effective technique to monitor the setting process and an alternative to the Vicat test.

McCarter et al. [31] used IS to monitor hydration kinetics and physico-chemical processes in concretes containing supplementary cementitious materials (blast furnace slag and fly ash). Four different hydration regions were identified from the electrical conductivity curve as a function of time. The regions were comprised as an initial region (i) a process of dissolution and precipitation of hydrates occurs, and an increase in conductivity is observed; a transition region (ii) hydrate

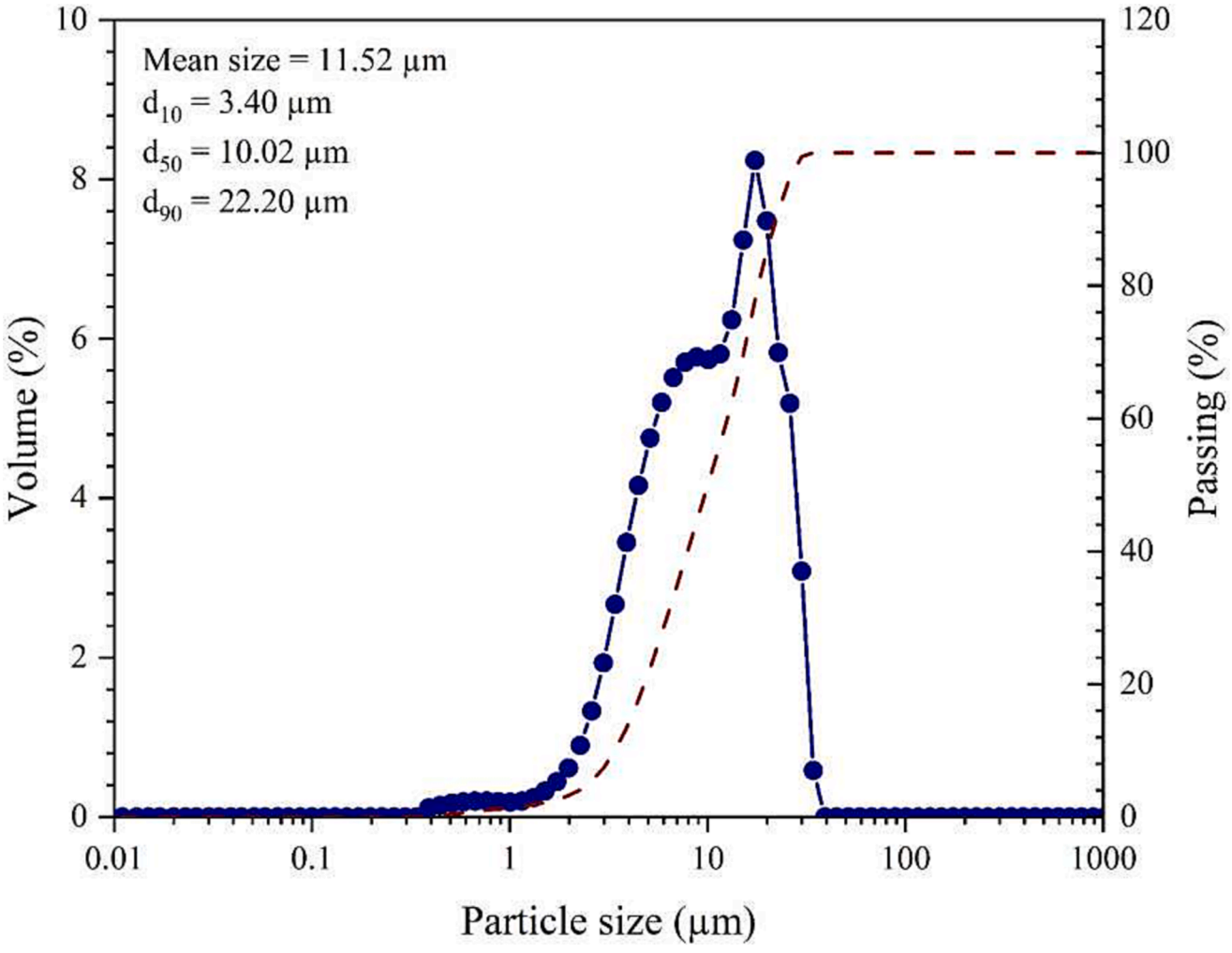

Fig. 1. Particle size distribution of anhydrous cement (CPV).

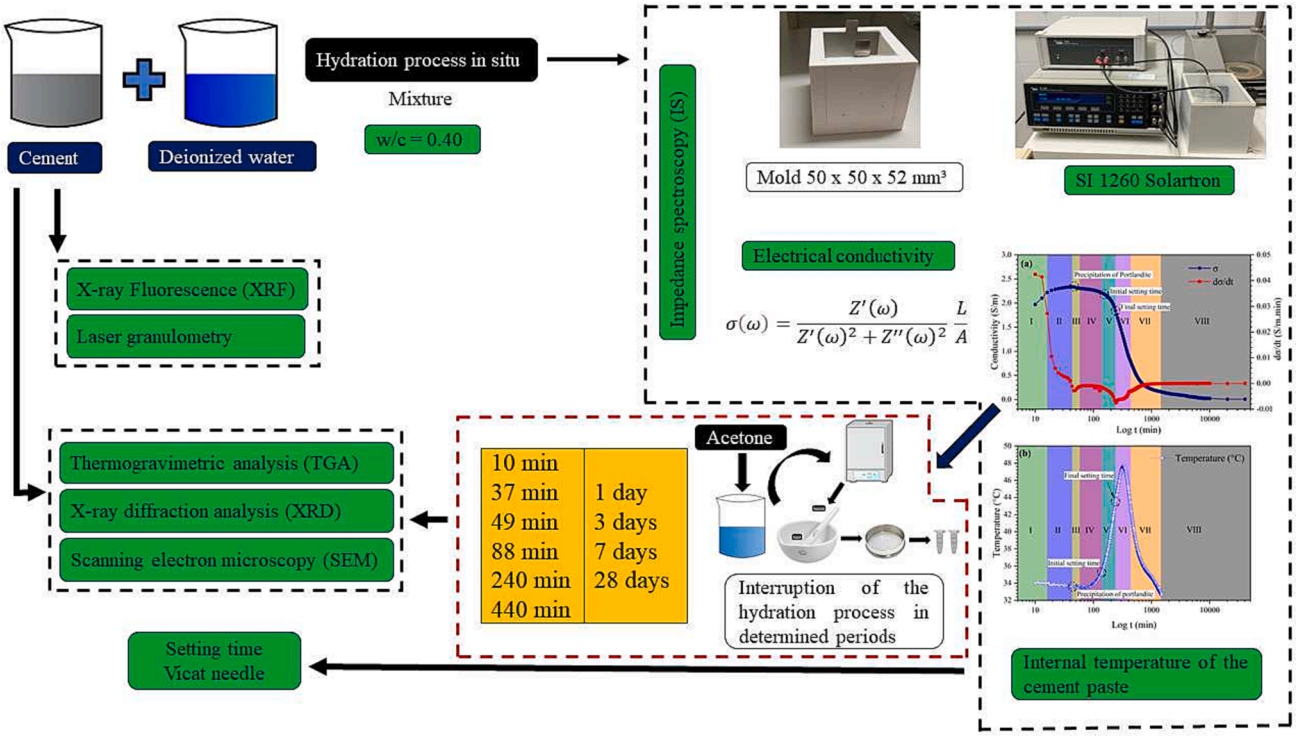

Fig. 2. Flowchart of the experimental program carried out in this study.

precipitation around the binder begins to dominate the dissolution process as a solid phase is developed and the conductivity gradually decreases; a region of rapid chemical activity (iii) intense precipitation of hydrates occurs, which results in the development of paste rigidity and the conductivity rapidly decreases; followed by a region of reduced chemical activity (iv) defined as the period of hardening and filling the pore network with products of hydration, the conductivity continues to decrease, albeit at a very low rate.

Suryanto et al. [25] employed IS and wet scanning electron microscopy (WetSEM) techniques to study the physico-chemical processes during the early hydration of Portland cement to provide additional information about the early stages of hydration and complementary information on hydrate formation. Six different hydration regions of Portland cement were identified from the electrical conductivity curve and its derivative, combined with WetSEM technology. The authors established, up to the maximum value of conductivity, two distinct regions in the hydration process, in which one region, the dissolution process occurs rapidly and the other region where the dissolution process continues predominant, albeit at a reduced rate. Furthermore, the authors observed that the reduction in conductivity after its maximum value corresponded to the beginning of precipitation of portlandite, confirmed by the WetSEM images.

However, the understanding of the processes that occur in the hydration of Portland cement from an electrical conductivity curve has not yet been fully elucidated, requiring further clarification and interpretation of the processes involved during hydration in specific periods of the conductivity curve, especially in the period belonging to the process of dissolution of the system and in the period after the maximum value of the conductivity. Therefore, further studies on the complex reactions of Portland cement using the IS technique should be carried out to understand the hydration processes not yet elucidated and establish the IS as a powerful tool in the study of complex hydration reactions of Portland cement.

In this way, this paper aims to provide a new perspective on the electrical conductivity curve of a Portland cement paste obtained from IS, in order to understand the different physico-chemical processes that occur during the hydration of Portland cement, mainly in the periods related to the dissolution process and after the maximum value of the conductivity. To support the electrical conductivity curve obtained from IS, measurements of time scale temperature, Vicat hardness, thermogravimetry (TG/DTG), X-ray diffractometry (XRD) and scanning electron microscopy (SEM) were performed.

2. Experimental program

2.1. Materials and preparation of cement pastes

The cement used to produce pastes was Brazilian Portland cement type CPV-ARI (cement type III in Standard ASTM C 150 [33]). This cement has high strength at early ages and does not contain pozzolan in its composition. The chemical composition and the particle size distribution of Portland cement were determined by X-ray fluorescence (Rigaku ZSX Primus IV) and laser granulometry (Mastersizer 2000 from Malvern Instruments) techniques and are presented in Table 1 and Fig. 1, respectively. The mineralogical composition, thermogravimetric analysis, and morphology of Portland cement were determined by the XRD, TG/DTG, and SEM techniques, respectively, and are presented and discussed in the supplementary material (Fig. S1 and Fig. S2).

The cement pastes were prepared using deionized water with a w/c ratio of 0.4 by mass. The samples were produced from the same cement bag to reduce material variability's influence on the results. The sample preparation process consisted of mechanically mixing the cement and water for 2 min. The pastes were produced in the laboratory at room temperature (26 ± 0.2 °C) and stored at 95 ± 2% relative humidity.

2.2. Test procedure

Besides the electrical conductivity curve obtained by the IS, measurements of XRD, TG/DTG, SEM, time scale temperature, and Vicat hardness were used to support the interpretation of the data obtained from the IS and in the identification of the processes involved during hydration. Fig. 2 illustrates a flowchart of the experimental program

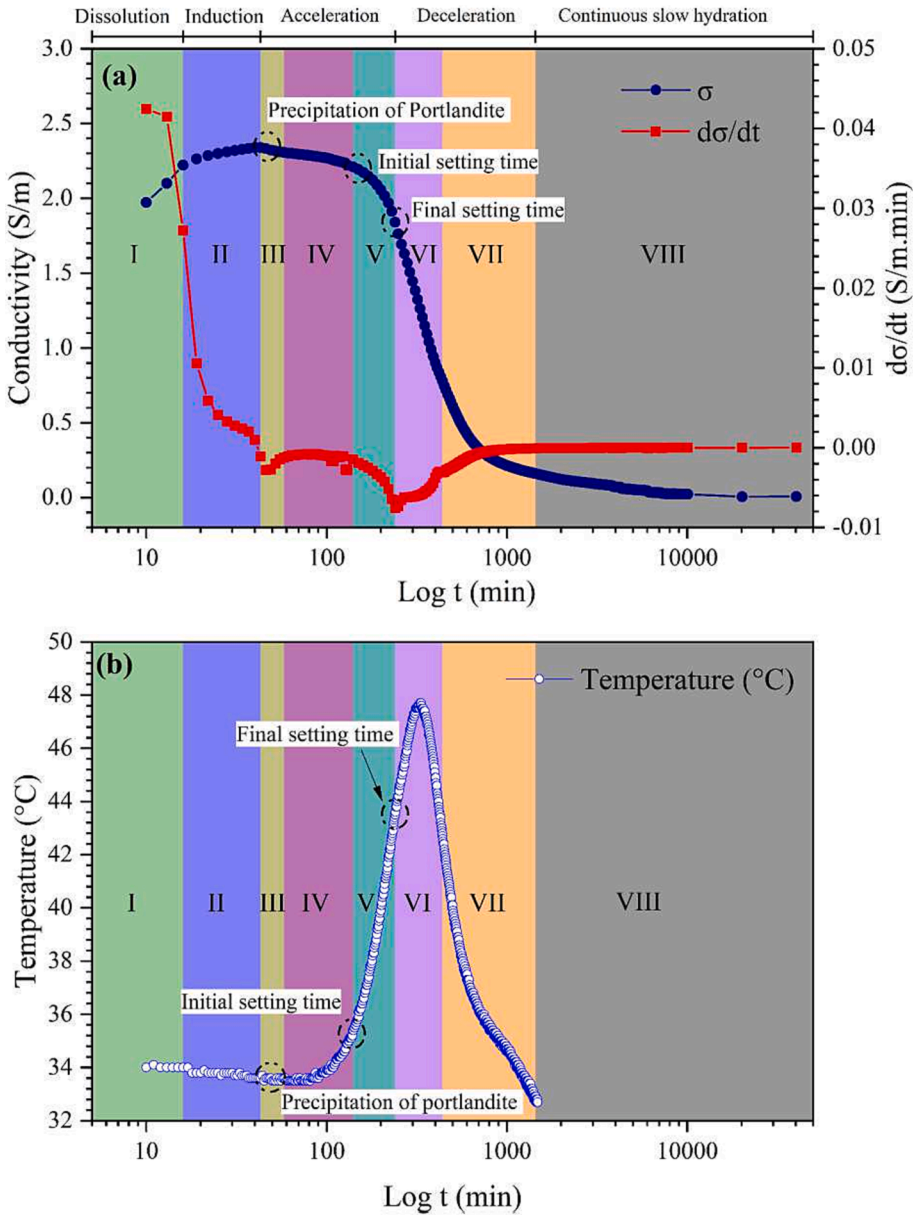

Fig. 3. (a) Conductivity, σ (100 kHz), and its derivative (dσ/dt) as a function of time for cement paste (CPV); and (b) Internal temperature of cement paste.

carried out.

2.2.1. Impedance spectroscopy

Impedance spectroscopy measurements were conducted as a function of cure time using a Solartron SI 1260 Impedance/Gain-Phase analyzer with a 1296 dielectric interface in the frequency range between 10^0 and 10^7 Hz employing 10 frequency points per decade. The applied voltage was 100 mV. Null test was adopted to eliminate the influence of mold and wires. To carry out the measurements, the pastes were molded in cubic molds of polyvinyl chloride in the dimensions 50 × 50 × 52 mm^3. Stainless steel plates (50 × 50 × 1 mm^3) with dimensions 10 × 10 × 1 mm^3 for connection were placed at the extremities of the mold to serve as electrodes (Fig. 2). During the entire measurement process, the system was kept in a controlled chamber with 95 ± 2% of humidity and a temperature of 26 ± 0.2 °C.

The Portland cement hydration was monitored from the first minutes of hydration up to 28 days of curing. Measurements were started 10 min after the contact of the binder with deionized water. Temporal monitoring was performed at predetermined intervals: every 3 min during the first 2 h; every 10 min until completing 24 h of reaction, and from then onwards, every 1 h until completing 7 days. After such periods, measurements were performed at 14 and 28 days of curing. In this interval, the samples were preserved in the respective molds with electrodes and kept in a chamber under the same measurement conditions.

The material impedance as a function of the angular frequency (ω) can be represented in its complex form as:

$$Z(\omega) = Z'(\omega) - iZ''(\omega) \quad (1)$$

where Z' (ω) is the real component (Ohm), Z'' (ω) is the imaginary component (Ohm), $i = \sqrt{-1}$ and $\omega = 2\pi f$, where f is the frequency of the applied electric field (Hz). As a function of the real and imaginary components of Z (ω), it is possible to determine the electrical conductivity σ (ω) of the material through Eq. (2) (information in the supplementary material):

$$\sigma(\omega) = \frac{Z'(\omega)}{Z'(\omega)^2 + Z''(\omega)^2}\frac{L}{A} \quad (2)$$

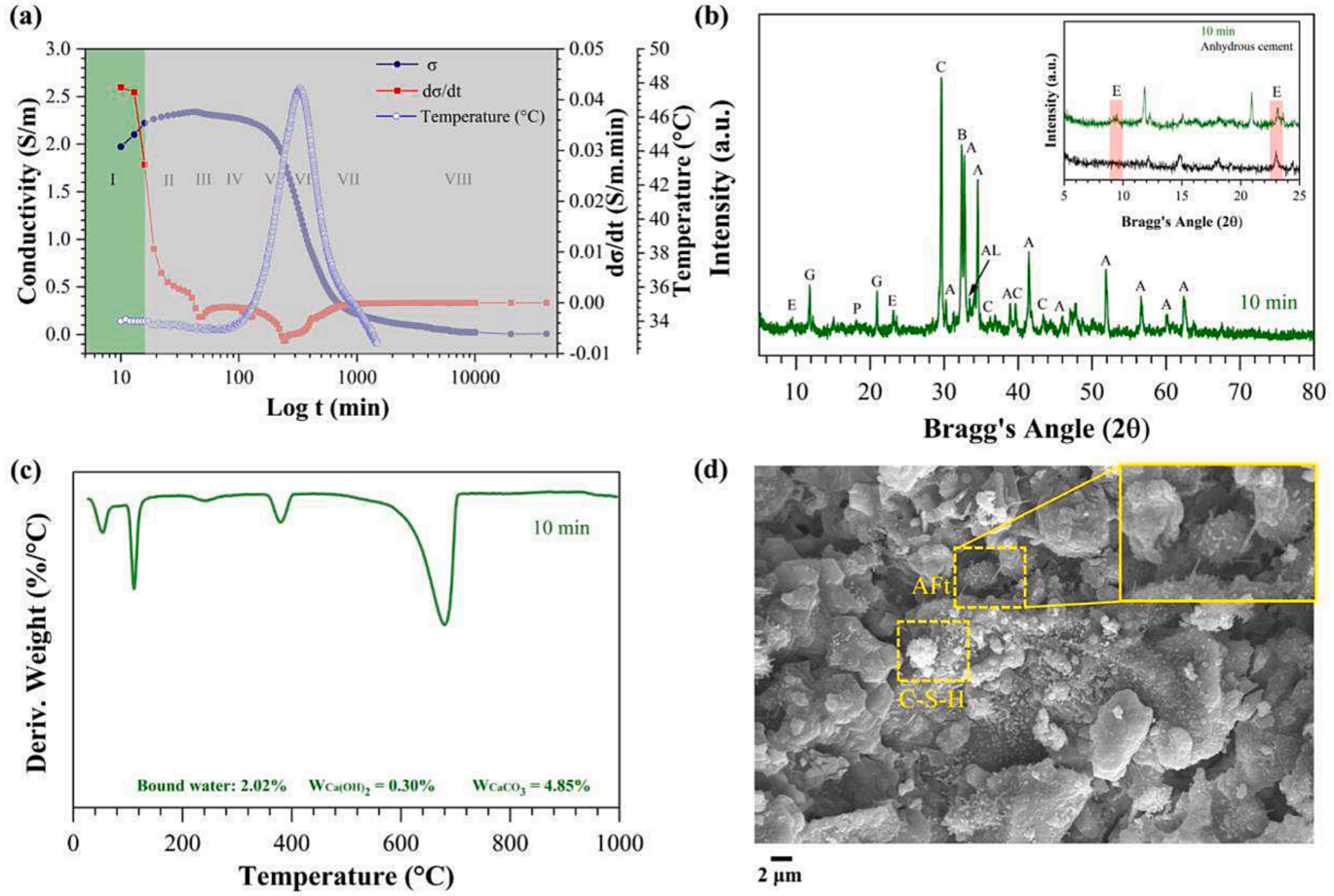

Fig. 4. Region I at 10 min of hydration (a) Conductivity (σ), derivative (dσ/dt) and internal temperature of cement paste in function of log t; (b) XRD diffractogram (A: Alite, C_3S; AL: Tricalcium aluminate, C_3A; B: Belite, C_2S; C: Calcite, $CaCO_3$; E: Ettringite, AFt; G: Calcium sulfate dihydrate, $CaSO_4{\cdot}2H_2O$; P: Calcium hydroxide; $Ca(OH)_2$); (c) DTG curve and (d) SEM image.

where L is the distance between the electrodes (m) and A is the area of the electrodes (m^2). The conductivity curve was presented at a frequency of 100 kHz to ensure the negligible influence of the electrode polarization and interfacial relaxation mechanisms, such as Maxwell-Wagner mechanisms, which become predominant at later ages of curing due to the development of microstructure as verified in the supplementary material (Fig. S4).

The internal temperature of the paste was recorded in situ every minute during the first 24 h of hydration using a Type K thermocouple via a data logger with a RS-232 interface.

2.2.2. Setting time

The setting time of the cement paste was determined using a Vicat apparatus according to ASTM C 191–19 [34]. The Vicat apparatus has a removable steel needle with a diameter of 1 mm and a length of not less than 50 mm, a movable rod of mass of 300 g, an internal diameter at the bottom of 70 mm, an internal diameter at the top of 60 mm and a height of 40 mm. Between penetration tests, the mold containing the paste was kept at a relative humidity of 95 ± 2%, being removed only at the time of the test.

2.2.3. Interruption of hydration processes

From the electrical conductivity curve data obtained from the IS technique, specific curing periods for each region were selected to perform the XRD, TG/DTG, and SEM measurements based on the inflections, maximum, and minimum of the electrical conductivity derivative curve.

For each selected curing age, small pieces of the sample or aliquot of the paste, depending on the age, were immersed/or dispersed in acetone to stop the hydration process. After 30 min, the samples were filtered and dried for 30 min in an oven at 60 °C. Subsequently, the samples were manually and gently macerated in an agate mortar, then sieved using a 75 µm sieve. Particles smaller than 75 µm were used in XRD and TG/DTG analyses. For SEM analysis, small pieces of the sample or aliquot of the paste were collected and immersed in acetone for 30 min and dried in an oven at 60 °C for 30 min.

2.2.4. Thermogravimetric analysis

Thermogravimetry measurements (TG/DTG) were carried out using SDTQ600 TA Instruments. Measurements were performed at a heating rate of 10 °C/min in the temperature range between 25 °C and 1000 °C using an inert nitrogen atmosphere (100 ml/min). The mass used in each sample was 10 ± 1 mg disposed of in alumina crucibles.

The amount of portlandite (% $Ca(OH)_2$) in the pastes were determined from the TG curves in the temperature range ~ 350 – 450 °C and calculated according to Eq. (3) [10]:

$$\%\ Ca(OH)_2 = W_{Ca(OH)_2} \times \frac{MM\,Ca(OH)_2}{MM\,H_2O} \quad (3)$$

where % $Ca(OH)_2$ is the amount of portlandite, $WCa(OH)_2$ is the percentage of mass loss related to dehydration of $Ca(OH)_2$ in this range, MM $Ca(OH)_2$ and MM H_2O represent the molecular mass of $Ca(OH)_2$ (74 g/mol) and water (18 g/mol), respectively. In turn, the calcium carbonate content (% $CaCO_3$) was quantified by the equation:

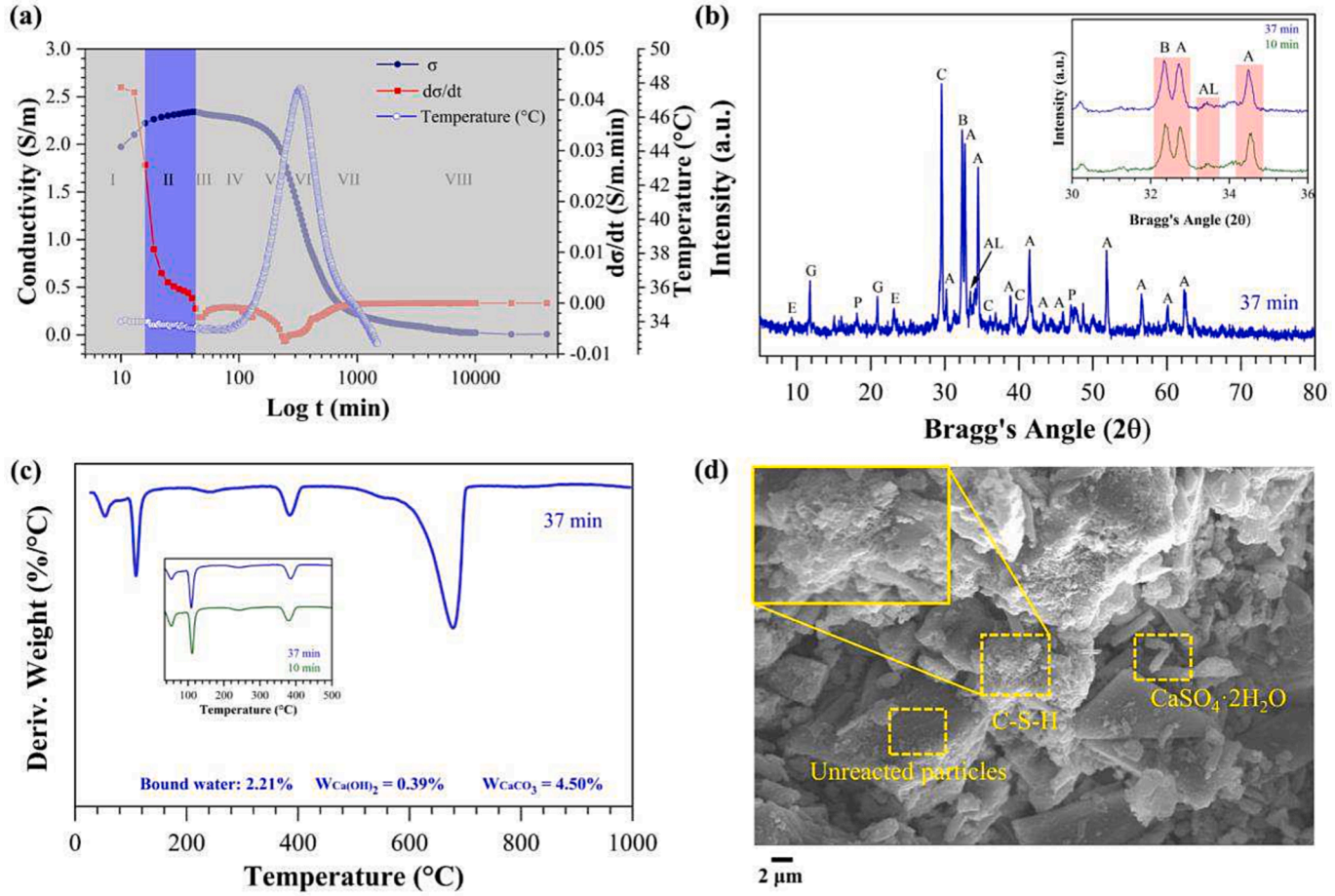

Fig. 5. Region II at 37 min of hydration (a) Conductivity (σ), derivative (dσ/dt) and internal temperature of cement paste in function of log t; (b) XRD diffractogram (A: Alite, C_3S; AL: Tricalcium aluminate, C_3A; B: Belite, C_2S; C: Calcite, $CaCO_3$; E: Ettringite, AFt; G: Calcium sulfate dihydrate, $CaSO_4{\cdot}2H_2O$; P: Calcium hydroxide; $Ca(OH)_2$); (c) DTG curve and (d) SEM image.

$$\%\ CaCO_3 = W_{CaCO_3} \times \frac{MM\ CaCO_3}{MM\ CO_2} \quad (4)$$

where % $CaCO_3$ is the percentage of carbonate material present in the composition, W_{CaCO_3} is the percentage of CO_2 released in the decomposition of $CaCO_3$, and MM $CaCO_3$ and MM CO_2 represent the molecular mass of $CaCO_3$ (100 g/mol) and CO_2 (44 g/mol), respectively.

The bound water content is commonly used to assess the degree of reaction in cementitious systems [35]. The percentage of bound water, that is, the water related to the hydrated products, was calculated based on the equation of Cruz et al. [36]:

$$\%\ \text{Bound water} = W_T - W_{Ca(OH)_2} - W_{CaCO_3} \quad (5)$$

where W_T is the percentage of total mass loss of the sample, $WCa(OH)_2$ is the percentage of water released in the decomposition of portlandite and $WCaCO_3$ is the percentage of CO_2 released in the decomposition of $CaCO_3$.

2.2.5. X-ray diffraction analysis

X-ray diffraction measurements were carried out using a Shimadzu XRD-6000 diffractometer (Cu-Kα, λ = 1.5418 Å) using a Ni filter. Measurements were performed in the range of 2θ = 5 – 80° using a voltage of 30 kV, current intensity of 40 mA, and 1°/min with a step size of 0.02°.

2.2.6. Scanning electron microscopy

The morphology of the anhydrous cement surface and the fractured surfaces of the paste were analyzed using a scanning electron microscope EVO LS15 – Zeiss coupled to an energy dispersive spectroscopy (EDX) detector. The samples were fixed on aluminum supports and coated with gold for the test (Quorum Q150T E). The thickness of the gold layer was on the order of 10 nm. Microscopy images were obtained in secondary electron mode, with the microscope operating at 20 kV.

3. Results and discussion

3.1. Characteristic points on the electrical conductivity curve

Fig. 3(a) illustrates the electrical conductivity curve (σ × log t) over 28 days of curing with its derivative (dσ/dt). The variations in the internal temperature of the Portland cement paste are illustrated in Fig. 3 (b). Through Fig. 3, based on the inflection points of the dσ/dt curve, it was possible to subdivide the electrical hydration curve into eight different regions (indicated I-VIII) to highlight the various stages of the Portland cement hydration process. From the subdivisions of the different hydration regions, in regions I-VII a curing age for each region was selected for the XRD, TG/DTG, and SEM analyses. In contrast, in region VIII three curing ages were selected, as illustrated in the flowchart of the experimental program (Fig. 2).

3.1.1. Discussion of hydration regions

3.1.1.1. Region I (0 to 16 min). In region I, upon mixing cement grains with water, ions (K^+, Na^+, SO_4^{2-}) are rapidly released from the surface of

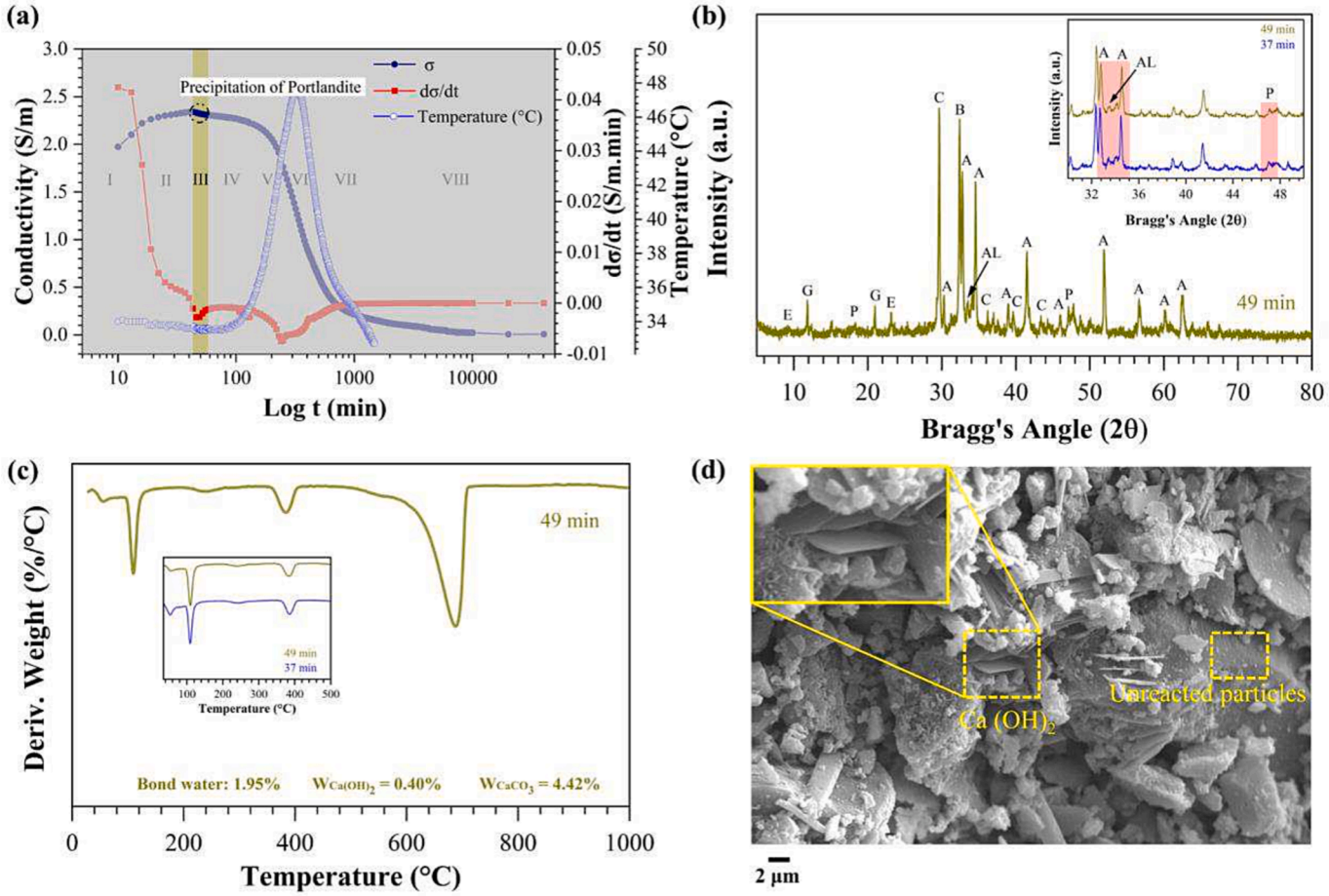

Fig. 6. Region III at 49 min of hydration (a) Conductivity (σ), derivative (dσ/dt) and internal temperature of cement paste in function of log t; (b) XRD diffractogram (A: Alite, C_3S; AL: Tricalcium aluminate, C_3A; B: Belite, C_2S; C: Calcite, $CaCO_3$; E: Ettringite, AFt; G: Calcium sulfate dihydrate, $CaSO_4{\cdot}2H_2O$; P: Calcium hydroxide; Ca $(OH)_2$); (c) DTG curve and (d) SEM image.

the cement grains, and the dissolution of clinker compounds such as C_3S, C_2S, C_3A, as well as calcium sulfate, begins [10]. An accentuated increase in σ was observed (up to 2.22 S/m) (Fig. 4(a)). This accentuated increase is associated with cement grains' dissolution process and release of alkaline ions, Ca^{2+}, SO_4^{2-} and OH^- into solution [28,37,38]. The paste at this time interval is in a fluid state with a colloidal dispersion. The concentration and mobility of the ions present in the solution are responsible for the increase in the conductivity of the paste. The dσ/dt presented positive values, and dσ/dt curve show a reduction trend, suggesting the existence of a competitive process: on the one hand, there was the ionic release in the medium, and, on the other hand, it can be observed the hydrates formation on the surfaces of the cement grains with consequent water consumption. The hydrates formation was observed in the XRD pattern (Fig. 4(b)), with the formation of AFt phases, at 2θ = 9.1° and 22.98° (PDF Card n° 41–1451), as well as in the TG measurement (Fig. 4(c)) through the bound water content and the decomposition pattern in the range 60–110 °C, which for the analyzed period, can be correlated both with the complete dehydration of calcium sulfate dihydrate in anhydrite as well as the presence of the AFt phase [35]. Fig. 4(c) shows a small amount of calcium hydroxide (1.22%) formed, probably, mianly due to the hydration of free CaO or C_3S of anhydrous Portland cement.

In the SEM image (Fig. 4(d)), the formation of some spongy structures characteristic of the early nucleation of calcium silicate hydrate (C-S-H), as well as of acicular structures resulting from the nucleation of AFt phases ($3CaO{\cdot}Al_2O_3{\cdot}3CaSO_4{\cdot}32H_2O$) were identified [3]. The nucleation and growth of hydrated phases such as C-S-H and AFt promote the fixation of Ca^{2+} and SO_4^{2-} ions and the consumption of free water in the system, reducing global electrical conductivity.

The rate at which the dissolution process occurs in this region is higher than the rate of formation of hydrated phases [4,25,39], thus ensuring a positive value for dσ/dt and an increasing behavior of σ; however, this difference between the rates decreases continuous with time, resulting in the reducing behaviour of the dσ/dt curve over this region.

3.1.1.2. Region II (16 to 43 min). Region II was characterized by a slight increase in the values of σ (when compared to region I), with its end assuming the maximum global value in the electrical conductivity curve (Fig. 5(a)). According to the literature, this maximum global value can be associated with the saturation of Ca^{2+} ions in the solution [22]. As mentioned previously, σ increase behavior indicates the predominance of the dissolution process with respect to the hydrates formation [25]. From 16 to 30 min, a significant reduction in the dσ/dt values was observed (from 0.027 to 0.003 S/m.min, about 10x). Juilland et al. [40] observed similar sharp reduction behavior in the alite dissolution rate in situations close to $Ca(OH)_2$ saturation. Nevertheless, from 30 min up to 37 min, the dσ/dt values continued to decrease, however, with a very low reduction with curing time.

In the literature, there is a divergence about the existence of region II. Some authors consider that this region belongs to the region I, where the dissolution process is predominant [20,28,31]. On the other hand, some authors consider region II distinct from the region I due to the less expressive increase in the σ values indicating the predominance of low

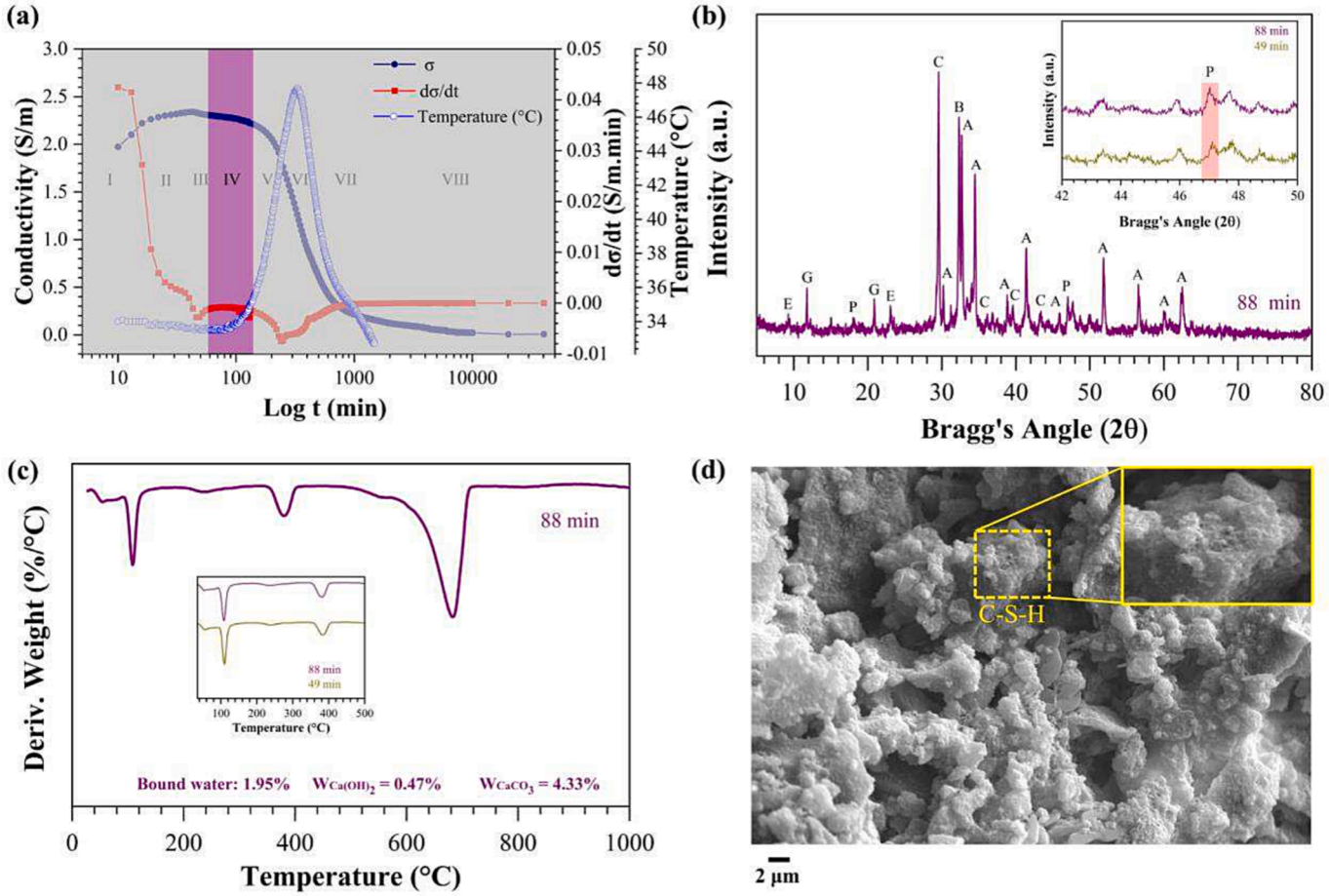

Fig. 7. Region IV at 88 min of hydration (a) Conductivity (σ), derivative (dσ/dt) and internal temperature of cement paste in function of log t; (b) XRD diffractogram (A: Alite, C_3S; B: Belite, C_2S; C: Calcite, $CaCO_3$; E: Ettringite, AFt; G: Calcium sulfate dihydrate, $CaSO_4{\cdot}2H_2O$; P: Calcium hydroxide; $Ca(OH)_2$); (c) DTG curve and (d) SEM image.

ions dissolution compared to the hydrated products formation [25,26].

X-ray diffraction patterns and the thermogravimetric curves of region II (Fig. 5(b) and Fig. 5(c), respectively) do not present significant differences with respect to the region I. In Fig. 5(d), SEM images highlighting the presence of C-S-H gels and prismatic structures of calcium sulfate dihydrate ($CaSO_4{\cdot}2H_2O$) were presented.

Hence, considering the above-mentioned statements and the obtained results, the authors consider adequate to differentiate region II from the region I due to its characteristic behavior: reduced dissolution rate observed in the σ curve, and a rapid reduction in the dσ/dt values with a very low reduction, tending towards a stabilization at the end of the region. Given such arguments, it seems plausible that region II deals directly with the induction period of Portland cement.

3.1.1.3. Region III (43 to 58 min). Region III was characterized as a region of short duration, in which a reduction in the values of σ (2.34 S/m to 2.31 S/m) and negative values of dσ/dt was observed (Fig. 6(a)). It indicates the prevalence of hydrated products formation in relation to the dissolution process, which continues occurring as confirmed by the reduction in the intensity of diffraction peaks of C_3S (32.72° and 34.52°) and C_3A (33.46°) when compared to region II (Fig. 6(b)). In the dσ/dt curve, a sharp local minimum of around 49 min was observed, indicating a formation/precipitation of hydrated products due to a rapid reduction of ions in the solution.

In the XRD pattern, no significant changes were observed in the portlandite diffraction pattern at $2\theta = 18.12°$ and $2\theta = 47.05°$ (Fig. 6(b)). In the same way, TG measurements do not present significant variations related to the $Ca(OH)_2$ content and hydrated compounds when compared to region II (Fig. 6(c)). In the SEM images (Fig. 6(d)), it was the first time (region III at 49 min) that the presence of portlandite (plate-like structures) could be observed. The results confirm the observations obtained by Suryanto et al. [25] for the same region, in which the authors evidenced the precipitation of portlandite. From these considerations, region III marks the start of the acceleration period from the portlandite formation.

The lack of information related to XRD patterns and thermogravimetric analysis demonstrates the importance of using IS as a powerful tool in studying Portland cement hydration.

3.1.1.4. Region IV (58 to 140 min). In this region, the conductivity presented a slow reduction, with σ values varying from 2.31 S/m to 2.21 S/m. In turn, dσ/dt presented negative values with small variations with curing time, resulting in a trend (unfulfilled) towards the formation of a plateau in the curve dσ/dt (Fig. 7(a)). The gradual reduction of σ values is certainly influenced by the enhanced formation and growth of hydrated products such as C-S-H gels, AFt, and portlandite, as confirmed in the measurements of XRD, TG, and observed in SEM image (Fig. 7). The formation and growth of these products result in the decrease of ions in the solution, generating discontinuous and tortuous paths from the microstructure in constitution, contributing to the conductivity reduction. Such facts are corroborated by the internal paste temperature (Fig. 7(a) and Fig. 3(b)), which was verified as an increased resumption. In the XRD pattern, a slight increase in the peak intensity of portlandite was evidenced at 47.05° at 88 min compared to region III (Fig. 7(b)),

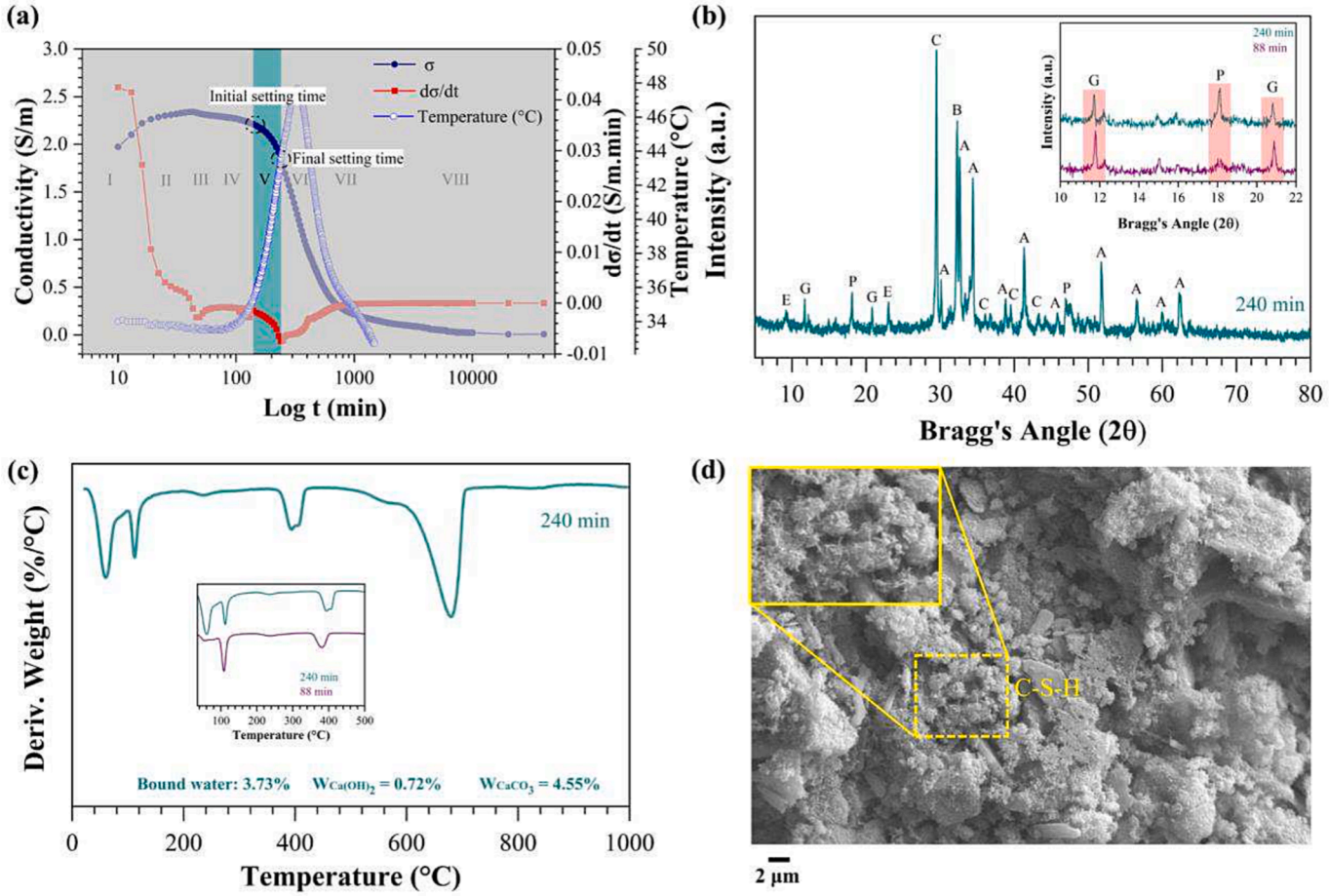

Fig. 8. Region V at 240 min of hydration (a) Conductivity (σ), derivative (dσ/dt) and internal temperature of cement paste in function of log t; (b) XRD diffractogram (A: Alite, C_3S; B: Belite, C_2S; C: Calcite, $CaCO_3$; E: Ettringite, AFt; G: Calcium sulfate dihydrate, $CaSO_4{\cdot}2H_2O$; P: Calcium hydroxide; $Ca(OH)_2$); (c) DTG curve and (d) SEM image.

indicating an increase in the amount and/or crystal organization this phase. In agreement, the TG measurement showed a higher dehydroxylation of $Ca(OH)_2$ (Fig. 7(c)), indicating a significant increase in portlandite content compared to previous stages. It was not observed an expressive variation in the content of the bound water for the region suggesting a slower formation of hydrated phases, corroborating with the temperature measurements.

The literature presents two divergent viewpoints for explaining and characterizing the period that follows the global peak of conductivity:

(1) Works that, by identifying the maximum peak of conductivity as the end of the dissolution period, characterize this region as belonging to the induction stage [20,23,31];
(2) Works that identify the maximum peak of conductivity as the region of initiation of the formation of portlandite and demarcate the later period as globally belonging to the acceleration stage, without its distinct identification [25,26,41].

Although the works characterized in item (2) do not recognize region IV as a particular region, the main characteristic that makes region IV a distinct region is the slight reduction in conductivity after the maximum of conductivity associated with small variations in the values of dσ/dt. The observation of this region does not seem to depend on the type of experimental apparatus used or the measurement methodology [20,23,25,26,31,41], although in works such as Taha et al. [26], it is possible to notice that dσ/dt values is dependent on the w/c ratio used in the pastes, tending to constant values at higher w/c ratios as used in this study, and to a reduction behavior with an almost linear trend in w/c ratios up to 0.35.

Although the identification of regions and their assignment to hydration stages may differ, in both cases (1) and (2), the authors based on thermal hydration curves (temperature or heat flow) to support their claims.

When considering the identification of the gradual formation of hydrated products, corroborated by XRD and TG measurements, which differ markedly from the previous stages characterized by the behavior of bound water and by the formation and development of phases such as portlandite, it becomes evident that Region IV belongs to the acceleration period, characterizing a distinct physical–chemical transition region that constitutes the initial moments of the acceleration period. During this stage, the paste remains in a semi-fluid state. In this, the dissolution reactions are resumed with the formation of hydrated phases and their precipitation with the beginning of the formation of the porous microstructure from the partial destabilization of the colloidal system and growth of the hydrated phases, which explains a region of distinct electrical characteristic, and among other factors, the dependence of the w/c ratio.

3.1.1.5. Region V (140 to 240 min). Region V was characterized by an accentuated reduction in conductivity, with the values of σ varying from 2.21 S/m to 1.84 S/m. The dσ/dt curve showed negative values, resulting in a global minimum at the end of the region at 240 min (Fig. 8 (a)). The accentuated reduction in conductivity was attributed to the formation and growth of hydration products, mainly to the nucleation

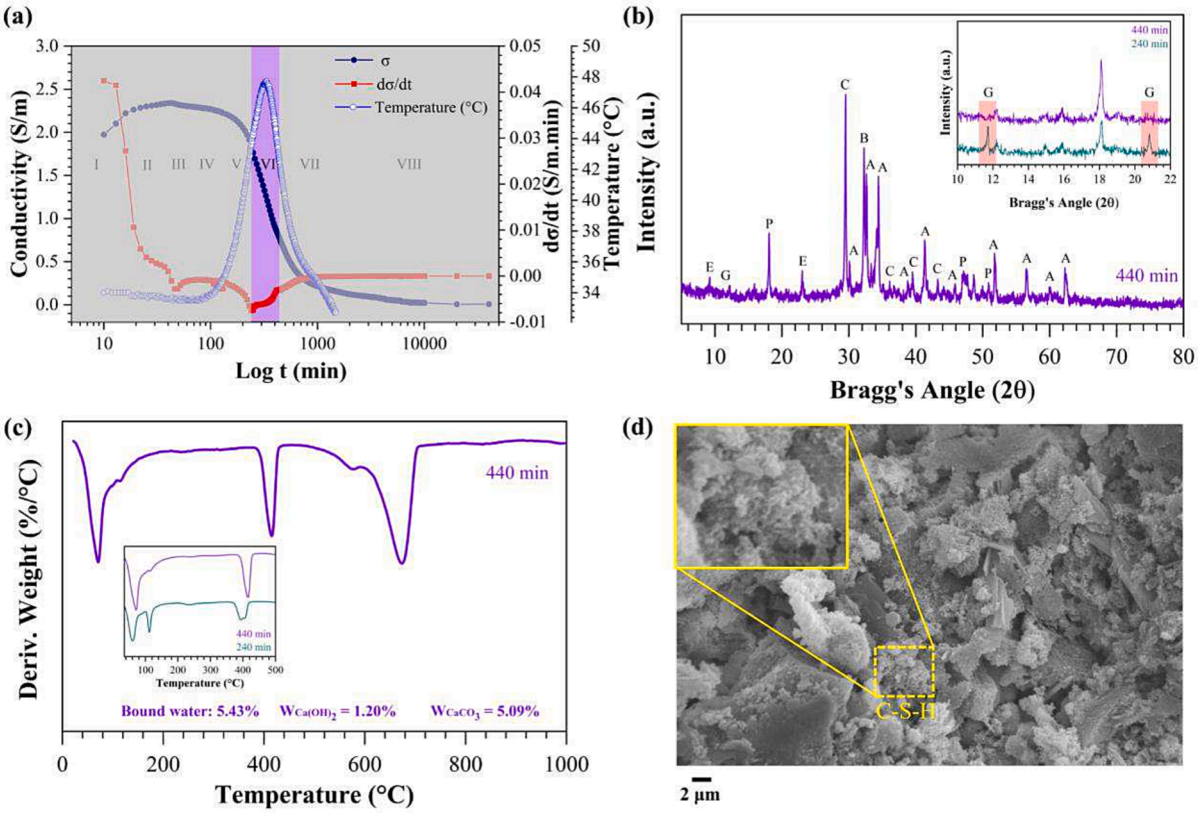

Fig. 9. Region VI at 440 min of hydration (a) Conductivity (σ), derivative (dσ/dt) and internal temperature of cement paste in function of log t; (b) XRD diffractogram (A: Alite, C_3S; B: Belite, C_2S; C: Calcite, $CaCO_3$; E: Ettringite, AFt; G: Calcium sulfate dihydrate, $CaSO_4{\cdot}2H_2O$; P: Calcium hydroxide; $Ca(OH)_2$); (c) DTG curve and (d) SEM image.

and growth of a "second stage" C-S-H [2], originated from a resumption of the chemical activity of the system from secondary dissolution reactions of C_3S that started in stage III. In corroboration, Fig. 3(b) showed an intense increase in system temperature, characteristic of the acceleration period. Vicat hardness measurements indicated the delimitation of the such region as the initial and final setting time of the paste. The values obtained in the Vicat test for the initial and final setting time of the paste were 148 min and 240 min, respectively. The maximum deviation of the values obtained between the IS and the Vicat test was approximately 5%, value also obtained by Sanish et al. [20], showing that the IS can be used to predict the setting time of Portland cement paste efficiently.

The formation and growth of hydration products were evidenced in the XRD pattern, in which an increase in peak intensity of 18.12° related to portlandite was observed (Fig. 8(b)), indicating a possible combination of a greater organization of the crystalline structure of the system from its growth. It was also possible to observe the beginning of the depletion of calcium sulfate, with the reduction in the intensity of the peaks at 11.82° and 20.94°. The TG measurement also confirmed the formation and growth of the hydrated products, showing an increase above 1% in the content of bound water and $Ca(OH)_2$ (Fig. 8(c)), as well as in the SEM image (Fig. 8(d)), which indicated a higher formation of C-S-H gel structures in relation to region IV. The growth of hydration products such as C-S-H gels, portlandite, and AFt caused the beginning of the solids interconnection and the consequent evolution of the microstructure formation, resulting in a decrease in the pore structure and in the volume of the liquid phase, which is associated with the final setting time of the paste and the consequent global minimum of the dσ/dt curve.

3.1.1.6. Region VI (240 to 440 min). A more accentuated reduction in conductivity characterized region VI compared to region V. The values of σ in this region showed a decrease of 57.79% (1.84 S/m to 0.78 S/m), while in region V the reduction was 16.70% (2.21 S/m to 1.84 S/m). The reduction in the σ value was mainly associated with constitution and growth of the hydrated products, as well as the reduction of free water from the constitution of the microstructure of the system and the reduction/narrowing of pores and capillary pores that predominate the global behavior. The dσ/dt presented negative values, however, the dσ/dt curve presented an increasing behavior, indicating an increase in dσ/dt over time (Fig. 9(a)). The negative values of dσ/dt show that phase constitution rates and the consequent consumption of free water and narrowing/closing of capillary pores predominates over ionic release processes that may be occurring in the system. The temperature measurement indicates a deceleration of the physico-chemical processes of Portland cement paste hydration after the global maximum of the T × t curve (Fig. 3(b)). The depletion of $CaSO_4$ observed by the reduction of the peaks at 11.82° and 20.94° in the XRD pattern (Fig. 9(b)) contributes to dσ/dt curve behavior, resulting in the initiation of phase conversion such as AFt to AFm, followed by the release of Ca^{2+} and SO_4^{2-} ions into the capillary pore network [25]. It was possible to observe a local minimum (*shoulder*) in the dσ/dt curve between 250 and 440 min (Fig. 9(a) and Fig. S5 in the supplementary material). The presence of this shoulder was mainly correlated with the formation of AFt phases from the beginning of the most accentuated consumption of $CaSO_4$ and the existence of secondary reactions of ionic release in the capillary pore system.

In the TG measurement (Fig. 9(c)), an increase of approximately 2% in portlandite and 1.7% in bound water was observed. Such findings are corroborated by SEM image (Fig. 9(d)), which indicated a growth of hydrated phases such as C-S-H gels and AFt, forming a denser and more compact microstructure in relation to the previous regions.

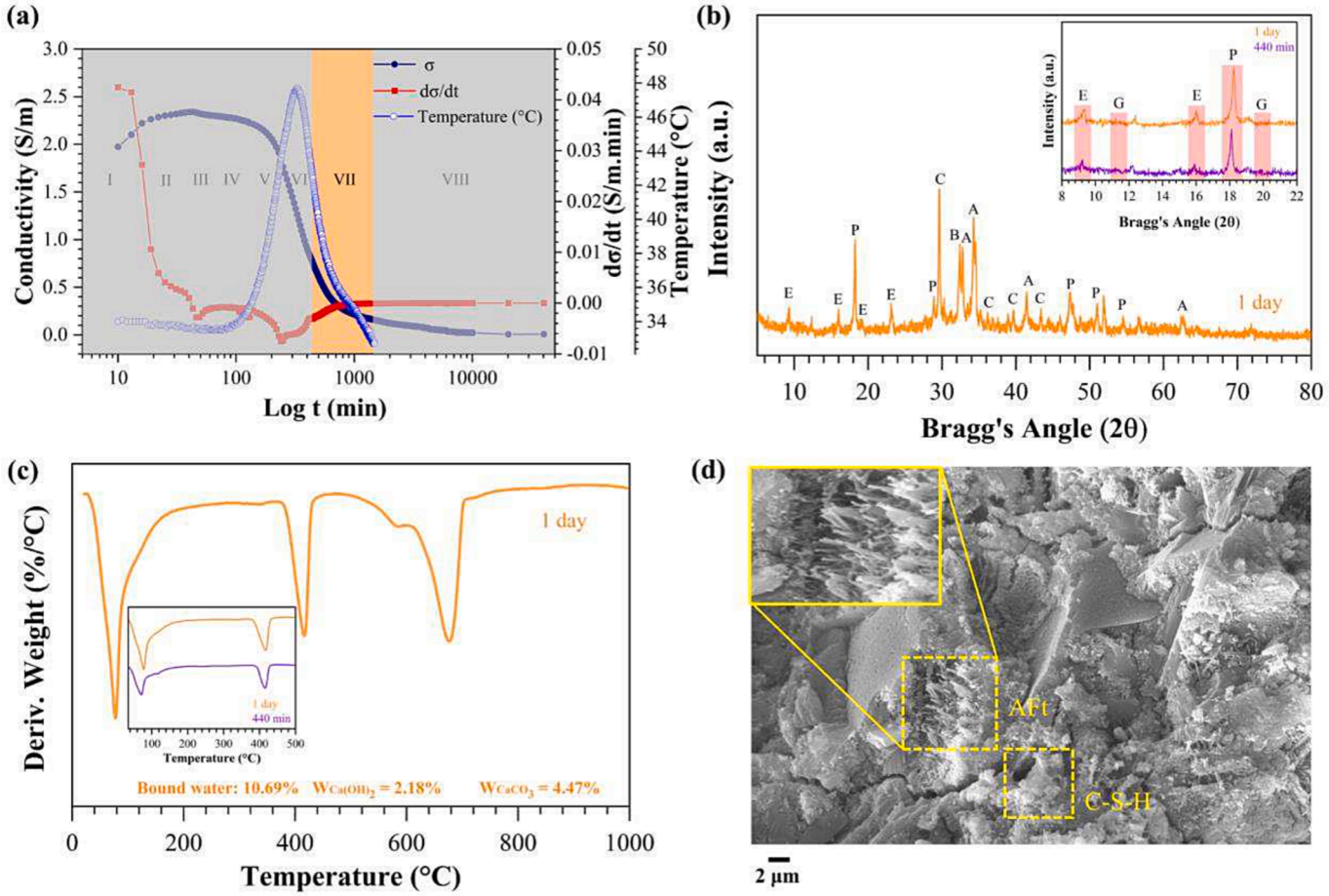

Fig. 10. Region VII at 1 day of hydration (a) Conductivity (σ), derivative (dσ/dt) and internal temperature of cement paste in function of log t; (b) XRD diffractogram (A: Alite, C_3S; B: Belite, C_2S; C: Calcite, $CaCO_3$; E: Ettringite, AFt; P: Calcium hydroxide; $Ca(OH)_2$); (c) DTG curve and (d) SEM image.

3.1.1.7. Region VII (440 to 1440 min). A gradual reduction in electrical conductivity characterized region VII, with σ values ranging from 0.78 S/m to 0.16 S/m (Fig. 10(a)). The dσ/dt showed negative values, however, dσ/dt curve show an increasing behavior, and along region VII the dσ/dt values showed a tendency of stabilization (dσ/dt≈0). The gradual reduction in σ values is related to the growth of the C-S-H gel, phases AFt phases and portlandite, and the conversion of part of AFt to AFm phases. The increasing behavior and consequent stabilization in the dσ/dt values indicate the reduction of the chemical activity of the system, characteristic of the deceleration period of Portland cement, and corroborated by the decrease of the internal temperature of the paste (Fig. 3(b)).

In the XRD pattern (Fig. 10(b)), calcium sulfate depletion was observed, illustrated by the disappearance of the peaks at 11.72° and 20.84° initiated in stage VI. The growth of AFt and portlandite phases was also evidenced, with an increase in peak intensity at 16.0° and 18.12°, respectively. In the TG measurement (Fig. 10(c)), an increase of approximately 5.2% in the combined water content and 1% in the amount of portlandite was observed, evidencing the growth of the hydrated products. These observations corroborate with the SEM image (Fig. 10(d)), which illustrated a higher densification of the C-S-H gel structure and the presence of AFt phases, indicating a less connected structure of the pore network through the interconnection of the solids [2,28].

3.1.1.8. Region VIII (1440 min -). Region VIII was characterized by the slow reduction in σ values with dσ/dt≈0 (Fig. 11(a)). This region marks the end of the sensitivity of impedance measurements for the adopted configuration. In this region, the hydration system is mainly controlled by diffusion processes, so the slow reduction of electrical conductivity is mainly associated with a slow changes in the microstructure of the paste still under development, correlated mainly with the growth of AFt and portlandite crystals, the conversion of part of the AFt to AFm and the densification of the C-S-H gel structure.

In the XRD pattern (Fig. 11(b)), an increase in the intensity of peaks related to AFt phases at 9.1°, 16.0° and 22.98° and portlandite at 18.12° and 47.1° was observed. AFm phases were also detected in the XRD pattern (PDF Card #83–1289) with peaks at 22.22° and 32.69°. In the TG measurement (Fig. 11(c)), it was possible to observe the slower formation of portlandite, as well as of the other hydrated products, caused mainly by the diffusion processes that govern this region and that directly reflect in the slower reduction of σ with dσ/dt≈0. The SEM images (Fig. 11(d) and Fig. S8 in the supplementary material) illustrated a more compact structure for the cement pastes, with a higher densification of the C-S-H gel structure and growth of AFt phases. The growth of hydrated phases at this stage influenced, in addition to the consumption of free water in the pore solution, the narrowing and increased tortuosity of the capillary pores of the system, contributing to this behavior.

3.2. Correlation of electrical conductivity, % $Ca(OH)_2$, % bound water

Fig. 12 illustrates the electrical conductivity curve as a function of the amount of portlandite, quantified by Eq. (3) (Fig. 12(a)-(b)), as well as the electrical conductivity curve as a function of mass loss of hydrated compounds (silicates, aluminates, and sulfates), quantified by Eq. (5)

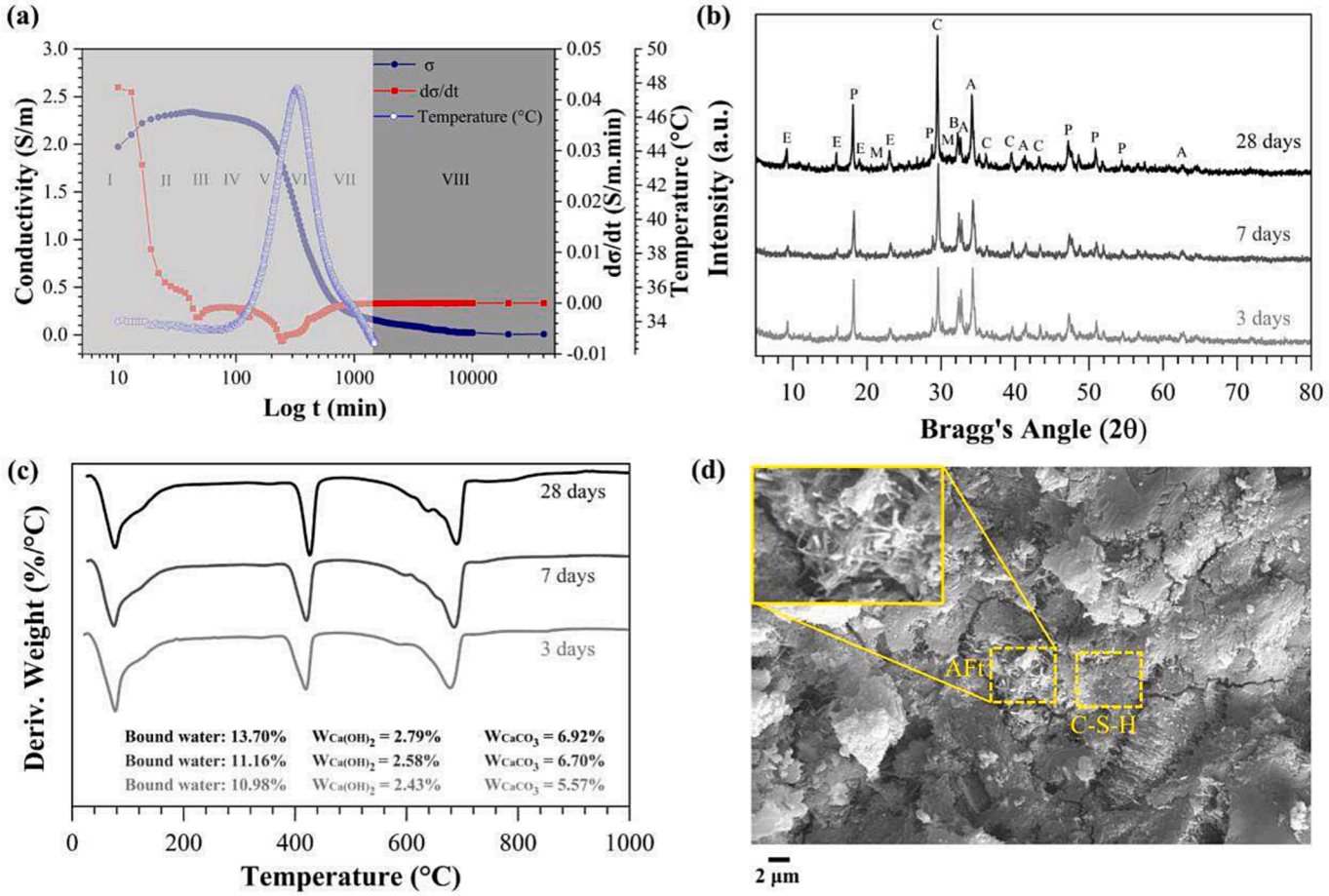

Fig. 11. Region VIII at 3, 7, and 28 days of hydration (a) Conductivity (σ), derivative (dσ/dt) and internal temperature of cement paste in function of log t; (b) XRD diffractogram (A: Alite, C_3S; B: Belite, C_2S; C: Calcite, $CaCO_3$; E: Ettringite, AFt; Monosulfate, AFm; P: Calcium hydroxide; $Ca(OH)_2$); (c) DTG curve and (d) SEM image.

(Fig. 12(c)-(d)). An exponential behavior can be predicted from the correlation, presenting a coefficient of determination of 0.96 and 0.97, respectively (Fig. 12(b)-(d)). The correlation shows that from the electrical conductivity curve, it was possible to follow the formation of portlandite and the formation of hydrated products in the microstructure over the curing time. The correlation is in accordance with the correlation performed by Liu et al. [42]. The authors obtained a coefficient of determination of 0.99 between the electrical conductivity curve and the chemical water content of the cement slurry.

3.3. Summary of main findings observed using IS

Table 2 is summarized the main events and characteristics observed using electrical conductivity curves for each region of Portland cement hydration.

4. Conclusion

New insights into the understanding of the electrical conductivity curve obtained from IS and hydration reactions of a Portland cement paste were the focus of this paper. Eight different hydration regions were identified from the electrical conductivity curve of the cement paste (σ × t) as well as its respective derivative (dσ/dt).

Two different regions were identified up to the maximum value of electrical conductivity (Region I and II), where dissolution reactions predominate over the formation of hydrated products. Region II showed a reduced rate of dissolution compared to region I, with region II corresponding to the induction period of Portland cement.

The reduction in conductivity observed in region III indicated the precipitation of portlandite from the removal of Ca^{2+} and OH^- ions in the solution.

Region IV was considered a physical–chemical transition region (the paste is in a semi-fluid state), which marks the initial moments of the acceleration period, from the slight reduction in conductivity and small variations in dσ/dt values.

Moreover, from the electrical conductivity curve, it was also possible to establish the initial and final setting time of the Portland cement paste (delimitation of region V). In general, IS proved to be a sensitive technique to monitor Portland cement hydration compared to conventional techniques, especially during early-age periods.

CRediT authorship contribution statement

M. Bortoletto: Data curation, Formal analysis, Investigation, Validation, Visualization, Writing – original draft. **A.O. Sanches:** Conceptualization, Data curation, Formal analysis, Investigation, Methodology, Writing – review & editing, Supervision. **J.A. Santos:** Data curation, Formal analysis, Investigation, Validation, Visualization. **R.G. da Silva:** Data curation, Formal analysis, Methodology, Visualization, Writing – original draft. **M.M. Tashima:** Conceptualization, Funding acquisition, Methodology, Project administration, Supervision, Writing – original draft, Writing – review & editing. **J. Payá:** Methodology, Validation, Visualization, Writing – review & editing. **L. Soriano:** Methodology, Validation, Visualization, Writing – review & editing. **M.V. Borrachero:**

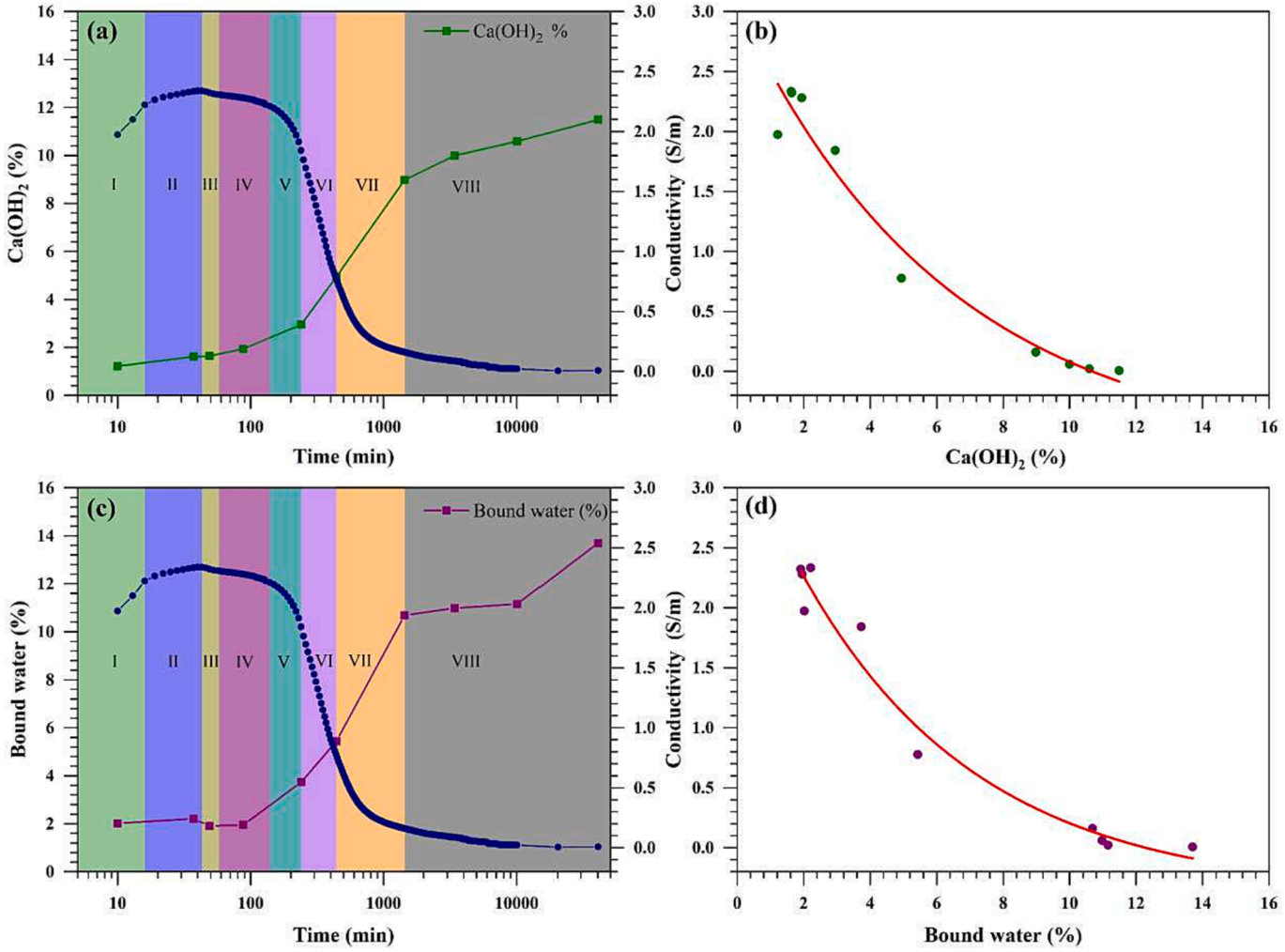

Fig. 12. (a) Evolution of amount of portlandite as a function of time; (b) correlation of the amount of portlandite with the electrical conductivity; (c) bound water content as a function of time and (d) correlation of the bound water content with the electrical conductivity. The electrical conductivity curve is presented to visualize the hydration regions in which the hydrates were quantified.

Table 2
Summary of the characteristics and key considerations of each region of the σ × t and dσ/dt × t curve.

Period of hydration	Regions of the σ × t and dσ/dt × t curves	Time	Characteristics	Key considerations
Dissolution	Region I	0—16 min	Accentuated increase of σ and positive values of dσ/dt, with dσ/dt showing a reduction behavior	Dissolution of ions and nucleation of hydrated phases (C-S-H gels and AFt)
Induction	Region II	16—43 min	Less expressive increase of σ and reduction in the values of dσ/dt	Low chemical activity, characterized by the induction period of Portland cement CPV
Acceleration	Region III	43—58 min	Reduction of σ and negative values of dσ/dt	Nucleation and precipitation of portlandite due to saturation of Ca^{2+} ions in the solution
	Region IV	58—140 min	Slight reduction of σ and negative values of dσ/dt tending to a plateau with the time	Transition region that marks the initial moments of the acceleration period (The paste is in a semi-fluid state)
	Region V	140—240 min	Accentuated reduction of σ and more negative values of dσ/dt	Formation and growth of hydration products, mainly to the nucleation and growth of a "second stage" C-S-H (Setting time of the paste)
Deceleration	Region VI	240—440 min	Accentuated reduction of σ and negative values of dσ/dt, with dσ/dt showing an increasing behavior.	Growth of hydrated products; formation of AFt phases and deceleration of the physico-chemical processes of hydration
	Region VII	440 min – 1440 min	Gradual reduction of σ and negative values of dσ/dt, with dσ/dt showing an increasing behavior and tendency of stabilization.	Reduction of the chemical activity of the system and the system becomes diffusion controlled
Continuous slow hydration	Region VIII	1440 min –	Slow reduction of σ and dσ/dt ≈ 0	Hydration systems are mainly controlled by diffusion

Methodology, Validation, Visualization, Writing – review & editing. **J.A. Malmonge:** Conceptualization, Data curation, Formal analysis, Investigation, Methodology, Writing – review & editing, Funding acquisition. **J.L. Akasaki:** Conceptualization, Funding acquisition, Methodology, Resources, Supervision.

Declaration of Competing Interest

The authors declare that they have no known competing financial interests or personal relationships that could have appeared to influence the work reported in this paper.

Data availability

Data will be made available on request.

Acknowledgments

The authors are grateful to Coordenação de Aperfeiçoamento de Pessoal de Nível Superior - Brazil (CAPES) – (Finance Code 001) and to Fundação de Amparo à Pesquisa do Estado de São Paulo – FAPESP (Project 2020/16325-0 and CEPID - CDMF 2013/07296-2) for the financial support and scholarship. Finally, M.M. Tashima wishes to thank the Spanish Ministry of Universities and the Universitat Politècnica de València for the grant "María Zambrano for attraction of international talent" funded by European Union-Next generation.

Appendix A. Supplementary data

Supplementary data to this article can be found online at https://doi.org/10.1016/j.conbuildmat.2023.133566.

References

[1] A.F. Sosa Gallardo, J.L. Provis, Electrochemical cell design and impedance spectroscopy of cement hydration, J. Mater. Sci. 56 (2021) 1203–1220, https://doi.org/10.1007/s10853-020-05397-6.
[2] J. Beaudoin, I. Odler, Hydration, Setting and Hardening of Portland Cement, in: Lea's Chem. Cem. Concr., 5th ed., Elsevier, 2019: pp. 157–250. https://doi.org/10.1016/B978-0-08-100773-0.00005-8.
[3] K.L. Scrivener, P. Juilland, P.J.M. Monteiro, Advances in understanding hydration of Portland cement, Cem. Concr. Res. 78 (2015) 38–56, https://doi.org/10.1016/j.cemconres.2015.05.025.
[4] M. Moradian, Q. Hu, M. Aboustait, M.T. Ley, J.C. Hanan, X. Xiao, V. Rose, R. Winarski, G.W. Scherer, Multi-scale observations of structure and chemical composition changes of portland cement systems during hydration, Constr. Build. Mater. 212 (2019) 486–499, https://doi.org/10.1016/j.conbuildmat.2019.04.013.
[5] K. Zhao, P. Zhang, S. Xue, S. Han, H.S. Müller, Y. Xiao, Y.u. Hu, L. Hao, L. Mei, Q. Li, Quasi-elastic neutron scattering (QENS) and its application for investigating the hydration of cement-based materials: State-of-the-art, Mater Charact 172 (2021) 110890.
[6] K.Y. Kim, T.S. Yun, J. Choo, D.H. Kang, H.S. Shin, Determination of air-void parameters of hardened cement-based materials using X-ray computed tomography, Constr. Build. Mater. 37 (2012) 93–101, https://doi.org/10.1016/j.conbuildmat.2012.07.012.
[7] A. Bogner, J. Link, M. Baum, M. Mahlbacher, T. Gil-Diaz, J. Lützenkirchen, T. Sowoidnich, F. Heberling, T. Schäfer, H.M. Ludwig, F. Dehn, H.S. Müller, M. Haist, Early hydration and microstructure formation of Portland cement paste studied by oscillation rheology, isothermal calorimetry, 1H NMR relaxometry, conductance and SAXS, Cem. Concr. Res. 130 (2020), 105977, https://doi.org/10.1016/j.cemconres.2020.105977.
[8] J. Zhang, L. Qin, Z. Li, Hydration monitoring of cement-based materials with resistivity and ultrasonic methods, Mater. Struct. Constr. 42 (2009) 15–24, https://doi.org/10.1617/s11527-008-9363-0.
[9] C.S. Deng, C. Breen, J. Yarwood, S. Habesch, J. Phipps, B. Craster, G. Maitland, Ageing of oilfield cement at high humidity: a combined FEG-ESEM and Raman microscopic investigation, J. Mater. Chem. 12 (2002) 3105–3112, https://doi.org/10.1039/b203127m.
[10] M.H. Maciel, G.S. Soares, R.C.d.O. Romano, M.A. Cincotto, Monitoring of Portland cement chemical reaction and quantification of the hydrated products by XRD and TG in function of the stoppage hydration technique, J. Therm. Anal. Calorim. 136 (3) (2019) 1269–1284.
[11] R. Wang, F. He, C. Shi, D. Zhang, C. Chen, L. Dai, AC impedance spectroscopy of cement - based materials: measurement and interpretation, Cem. Concr. Compos. 131 (2022), 104591, https://doi.org/10.1016/j.cemconcomp.2022.104591.
[12] D. Jansen, F. Goetz-Neunhoeffer, B. Lothenbach, J. Neubauer, The early hydration of Ordinary Portland Cement (OPC): An approach comparing measured heat flow with calculated heat flow from QXRD, Cem. Concr. Res. 42 (2012) 134–138, https://doi.org/10.1016/j.cemconres.2011.09.001.
[13] M. Wu, S. Sui, Y. Zhang, Y. Jia, W. She, Z. Liu, Y. Yang, Analyzing the filler and activity effect of fly ash and slag on the early hydration of blended cement based on calorimetric test, Constr. Build. Mater. 276 (2021), 122201, https://doi.org/10.1016/j.conbuildmat.2020.122201.
[14] T. Dorn, O. Blask, D. Stephan, Acceleration of cement hydration – A review of the working mechanisms, effects on setting time, and compressive strength development of accelerating admixtures, Constr. Build. Mater. 323 (2022) 126554.
[15] X. Zhang, X.Z. Ding, C.K. Ong, B.T.G. Tan, J. Yang, Dielectric and electrical properties of ordinary Portland cement and slag cement in the early hydration period, J. Mater. Sci. 31 (1996) 1345–1352, https://doi.org/10.1007/BF00353116.
[16] W.J. McCarter, S. Garvin, N. Bouzid, Impedance measurements on cement paste, J. Mater. Sci. Lett. 7 (10) (1988) 1056–1057.
[17] X. Hu, C. Shi, X. Liu, J. Zhang, G. de Schutter, A review on microstructural characterization of cement-based materials by AC impedance spectroscopy, Cem. Concr. Compos. 100 (2019) 1–14, https://doi.org/10.1016/j.cemconcomp.2019.03.018.
[18] S.W. Tang, H.G. Zhu, Z.J. Li, E. Chen, H.Y. Shao, Hydration stage identification and phase transformation of calcium sulfoaluminate cement at early age, Constr. Build. Mater. 75 (2015) 11–18, https://doi.org/10.1016/j.conbuildmat.2014.11.006.
[19] J. Zhang, F. Zheng, Z. Liu, S. Hong, B. Dong, F. Xing, Nondestructive monitoring on hydration behavior of cement pastes via the electrochemical impedance spectroscopy method, Meas. J. Int. Meas. Confed. 185 (2021), 109884, https://doi.org/10.1016/j.measurement.2021.109884.
[20] K.B. Sanish, N. Neithalath, M. Santhanam, Monitoring the evolution of material structure in cement pastes and concretes using electrical property measurements, Constr. Build. Mater. 49 (2013) 288–297, https://doi.org/10.1016/j.conbuildmat.2013.08.038.
[21] A.F. Sosa Gallardo, Electrochemical impedance spectroscopy as a probe of cement hydration and microstructure, University of Sheffield, 2020.
[22] S.W. Tang, X.H. Cai, Z. He, W. Zhou, H.Y. Shao, Z.J. Li, T. Wu, E. Chen, The review of early hydration of cement-based materials by electrical methods, Constr. Build. Mater. 146 (2017) 15–29, https://doi.org/10.1016/j.conbuildmat.2017.04.073.
[23] M. Perez-Pena, D.M. Roy, F.D. Tamas, Influence of chemical composition and inorganic admixtures on the electrical conductivity of hydrating cement pastes, J. Mater. Res. 4 (1989) 215–223, https://doi.org/10.1557/JMR.1989.0215.
[24] L. Chi, W. Li, Z. Li, Z. Wang, S. Lu, Q. Liu, Investigation of the hydration properties of cement with EDTA by alternative current impedance spectroscopy, Cem. Concr. Compos. 126 (2022), 104365, https://doi.org/10.1016/j.cemconcomp.2021.104365.
[25] B. Suryanto, J.O. Buckman, W.J. McCarter, H. Taha, In-situ dynamic WetSEM imaging and electrical impedance measurements on Portland cement during early hydration, Mater Charact 142 (2018) 86–100, https://doi.org/10.1016/j.matchar.2018.05.028.
[26] H.M. Taha, W.J. McCarter, B. Suryanto, G. Starrs, Frequency- and time-domain dependency of electrical properties of cement-based materials during early hydration, Adv. Civ. Eng. Mater. 6 (2017) 65–83, https://doi.org/10.1520/ACEM20160057.
[27] R.K. Manchiryal, N. Neithalath, Analysis of the influence of material parameters on electrical conductivity of cement pastes and concretes, Mag. Concr. Res. 61 (2009) 257–270, https://doi.org/10.1680/macr.2008.00064.
[28] N. Schwarz, M. DuBois, N. Neithalath, Electrical conductivity based characterization of plain and coarse glass powder modified cement pastes, Cem. Concr. Compos. 29 (2007) 656–666, https://doi.org/10.1016/j.cemconcomp.2007.05.005.
[29] Z. He, R. Cai, E. Chen, S. Tang, The investigation of early hydration and pore structure for limestone powder wastes blended cement pastes, Constr. Build. Mater. 229 (2019), 116923, https://doi.org/10.1016/j.conbuildmat.2019.116923.
[30] B.J. Christensen, T. Coverdale, R.A. Olson, S.J. Ford, E.J. Garboczi, H.M. Jennings, T.O. Mason, Impedance spectroscopy of hydrating cement-based materials: measurement, interpretation, and application, J. Am. Ceram. Soc. 77 (1994) 2789–2804, https://doi.org/10.1111/j.1151-2916.1994.tb04507.x.
[31] W.J. McCarter, T.M. Chrisp, G. Starrs, A. Adamson, P.A.M. Basheer, S. V. Nanukuttan, S. Srinivasan, C. Green, Characterization of physio-chemical processes and hydration kinetics in concretes containing supplementary cementitious materials using electrical property measurements, Cem. Concr. Res. 50 (2013) 26–33, https://doi.org/10.1016/j.cemconres.2013.03.008.
[32] T. Huang, Q. Yuan, S. Zuo, B. Li, Q. Wu, Y., Xie, Evaluation of microstructural changes in fresh cement paste using AC impedance spectroscopy vs. oscillation rheology and 1 H NMR relaxometry, Cem. Concr. Res. 149 (2021), 106556, https://doi.org/10.1016/j.cemconres.2021.106556.
[33] ASTM International, Standard Specification for Portland Cement, (2022) 1–9. https://doi.org/10.1520/C0150.
[34] ASTM International, Standard test methods for Time of Setting of Hydraulic Cement by Vicat Needle, (2019) 1–8. https://doi.org/10.1520/C0191-19.2.
[35] K. Scrivener, R. Snellings, B. Lothenbach, A practical guide to microstructural analysis of cementitious materials, Spon Press Boca Raton (2016), https://doi.org/10.1201/b19074.
[36] J.M. Cruz, I.C. Fita, L. Soriano, J. Payá, M.V. Borrachero, The use of electrical impedance spectroscopy for monitoring the hydration products of Portland cement mortars with high percentage of pozzolans, Cem. Concr. Res. 50 (2013) 51–61, https://doi.org/10.1016/j.cemconres.2013.03.019.

[37] T.M. Salem, Electrical conductivity and rheological properties of ordinary Portland cement-silica fume and calcium hydroxide-silica fume pastes, Cem. Concr. Res. 32 (2002) 1473–1481, https://doi.org/10.1016/S0008-8846(02)00809-8.
[38] S.W. Tang, Z.J. Li, H.Y. Shao, E. Chen, Characterization of early-age hydration process of cement pastes based on impedance measurement, Constr. Build. Mater. 68 (2014) 491–500, https://doi.org/10.1016/j.conbuildmat.2014.07.009.
[39] Q. Hu, M. Aboustait, T. Kim, M.T. Ley, J.W. Bullard, G. Scherer, J.C. Hanan, V. Rose, R. Winarski, J. Gelb, Direct measurements of 3d structure, chemistry and mass density during the induction period of C3s hydration, Cem. Concr. Res. 89 (2016) 14–26, https://doi.org/10.1016/j.cemconres.2016.07.008.
[40] P. Juilland, E. Gallucci, R. Flatt, K. Scrivener, Dissolution theory applied to the induction period in alite hydration, Cem. Concr. Res. 40 (2010) 831–844, https://doi.org/10.1016/j.cemconres.2010.01.012.
[41] F.D. Tamás, Electrical conductivity of cement pastes, Cem. Concr. Res. 12 (1) (1982) 115–120.
[42] K. Liu, X. Cheng, J. Li, X. Gao, Y. Cao, X. Guo, J. Zhuang, C. Zhang, Effects of microstructure and pore water on electrical conductivity of cement slurry during early hydration, Compos. B Eng. 177 (2019), 107435, https://doi.org/10.1016/j.compositesb.2019.107435.